

## Robust chaos in a model of the electroencephalogram: Implications for brain dynamics

Mathew P. Dafilis, David T. J. Liley, and Peter J. Cadusch

*Centre for Intelligent Systems and Complex Processes, School of Biophysical Sciences and Electrical Engineering, Swinburne University of Technology, Hawthorn Vic 3122, Australia*

(Received 13 December 2000; accepted 15 June 2001; published 20 August 2001)

Various techniques designed to extract nonlinear characteristics from experimental time series have provided no clear evidence as to whether the electroencephalogram (EEG) is chaotic. Compounding the lack of firm experimental evidence is the paucity of physiologically plausible theories of EEG that are capable of supporting nonlinear and chaotic dynamics. Here we provide evidence for the existence of chaotic dynamics in a neurophysiologically plausible continuum theory of electrocortical activity and show that the set of parameter values supporting chaos within parameter space has positive measure and exhibits fat fractal scaling. © 2001 American Institute of Physics. [DOI: 10.1063/1.1394193]

**Since the introduction of techniques to extract nonlinear characteristics from experimental time series an open question in brain dynamics has been whether the brain does indeed show signs of nonlinear or even chaotic activity. The electroencephalogram (EEG) is a signal recorded by scalp electrodes reflecting the synchronous activity of many millions of neurones. Experimental analyses of the EEG to date have failed to show clear evidence of chaotic activity. Here we consider the question from a theoretical viewpoint, presenting evidence confirming the existence of chaotic dynamics in a biologically realistic model of brain electrical activity, also suggesting, however, that a direct observation of chaotic activity in the electroencephalogram is unlikely. We discuss the implications of this work for Freeman's theory of perceptual neurodynamics.**

### INTRODUCTION

One of the few coherent attempts to clearly relate the EEG to macroscopic cortical dynamics is Freeman's work on olfactory perception and palaeocortical EEG which suggests that the existence of chaos in cortical neurodynamics is the very property that makes perception possible, giving brains their ability to respond flexibly and coherently to perceptual stimuli.<sup>1,2</sup> The neocortical electroencephalogram is far more complicated than its palaeocortical counterpart.<sup>3</sup> Notwithstanding this a considerable amount of experimental and theoretical work has been performed in an attempt to understand neocortical neural dynamics and to determine whether the human neocortical EEG shows signs of chaos. Other well regarded macroscopic theories of EEG<sup>4-8</sup> do not predict and in some cases do not allow the expression of chaotic dynamics at either macrocolumnar or whole-brain scales. Further the considerable body of experimental work in this area has provided largely equivocal results, with the continued refinement of nonlinear time series analysis techniques leaving many questions unresolved.<sup>9</sup>

Here we provide theoretical evidence for chaotic dynam-

ics underlying the human EEG, based on the simplest theory of neocortical EEG that is consistent with known anatomy and physiology. We find support for the chaotic gamma band activity required by Freeman's theory of perceptual dynamics and show evidence for extensive chaos under widespread parametric variation.

### THEORY

It is well established that the electroencephalogram (EEG) is directly proportional to the local field potential recorded by electrodes on the brain's surface.<sup>10</sup> Furthermore, one single EEG electrode placed on the scalp records the aggregate electrical activity from up to 6 cm<sup>2</sup> of brain surface, and hence many millions of neurones.<sup>11</sup> With such large numbers, modeling the system via a discrete enumeration of these neurones becomes infeasible—instead a continuum approach is warranted where the neocortex and its dynamics are treated as a continuous sheet of neurones whose activity varies with time.

Continuum models of neocortex to date fall into two broad classes: those which describe the dynamics of a neocortical macrocolumn, consisting of anywhere between 40 000 and 100 000 neurones in a small volume of neocortex (referred to as local models), and those which describe the activity of the whole neocortical mantle (referred to as global models).<sup>4</sup> The model we consider here is a local model derived from the more general global theory of Liley *et al.*<sup>12</sup> The model examined comes from the simplest physiologically and anatomically consistent theory of electrocortical dynamics, whose parametrization is entirely amenable to experiment independent of this particular theory.

The model considers the behavior of the mean soma membrane potential of two functionally distinct neural populations. A population of excitatory neurones is reciprocally connected to a population of inhibitory neurones, with excitatory feedback to the excitatory population and inhibitory feedback to the inhibitory population and with external excitatory and inhibitory inputs to each population. All connec-

tions between populations and inputs are modeled on the dynamics of fast-acting synapses.<sup>12</sup> All parameter values used are within known physiological bounds. The main state variable for the excitatory population (the mean soma membrane potential of the population) is directly proportional to the local field potential of the neural aggregate, which predominates in the scalp-recorded electroencephalogram.<sup>10</sup>

The model is formulated as a set of coupled first and second order nonlinear ordinary differential equations (ODEs), which we solve numerically. The equations which comprise the model are

$$\tau_e \frac{dh_e}{dt} = (h_{er} - h_e) + \frac{h_{eeq} - h_e}{|h_{eeq} - h_{er}|} I_{ee} + \frac{h_{ieq} - h_e}{|h_{ieq} - h_{er}|} I_{ie}, \quad (1)$$

$$\tau_i \frac{dh_i}{dt} = (h_{ir} - h_i) + \frac{h_{eeq} - h_i}{|h_{eeq} - h_{ir}|} I_{ei} + \frac{h_{ieq} - h_i}{|h_{ieq} - h_{ir}|} I_{ii}, \quad (2)$$

$$\frac{d^2 I_{ee}}{dt^2} + 2a \frac{dI_{ee}}{dt} + a^2 I_{ee} = Aae\{N_{ee}S_e(h_e) + p_{ee}\}, \quad (3)$$

$$\frac{d^2 I_{ie}}{dt^2} + 2b \frac{dI_{ie}}{dt} + b^2 I_{ie} = Bbe\{N_{ie}S_i(h_i) + p_{ie}\}, \quad (4)$$

$$\frac{d^2 I_{ei}}{dt^2} + 2a \frac{dI_{ei}}{dt} + a^2 I_{ei} = Aae\{N_{ei}S_e(h_e) + p_{ei}\}, \quad (5)$$

$$\frac{d^2 I_{ii}}{dt^2} + 2b \frac{dI_{ii}}{dt} + b^2 I_{ii} = Bbe\{N_{ii}S_i(h_i) + p_{ii}\}, \quad (6)$$

where

$$S_q(h_q) = q_{\max} / (1 + \exp(-\sqrt{2}(h_q - \theta_q)/s_q)): \quad q = e, i. \quad (7)$$

Equations (1) and (2) describe the temporal evolution of  $h_e$  and  $h_i$ , the mean soma membrane potentials of the excitatory and inhibitory populations, respectively. Equations (3)–(6) describe the temporal evolution of the “synaptic” activity, with the  $S$  functions converting the mean soma membrane potential of the respective population into an equivalent mean firing rate, which then acts as a drive to the second order “synapse” described by the left-hand-sides of these equations. These equations represent a spatially homogeneous form of a more complete model of spatio-temporal electrocortical dynamics.<sup>12</sup>

Parameters  $A$  and  $B$  are the excitatory and inhibitory population postsynaptic potential peak amplitudes, with  $a$  and  $b$  the respective synaptic rate constants, with the multiplier  $e$  being the base of natural logarithms. Population membrane time constants are given by  $\tau_e, \tau_i$ , with resting and equilibrium potentials given by  $h_{er}, h_{ir}$ , and  $h_{eeq}$  and  $h_{ieq}$ . Excitatory inputs to the respective populations are given by  $p_{ee}$  and  $p_{ei}$ , with inhibitory inputs given by  $p_{ie}$  and  $p_{ii}$ . Excitatory neurones each receive a total of  $N_{ee}$  and  $N_{ie}$  synapses from nearby excitatory and inhibitory neurones, respectively, with inhibitory neurones receiving a total  $N_{ei}$  and  $N_{ii}$  synapses. The excitatory and inhibitory population firing thresholds and standard deviations for these thresholds are given by  $\theta_e, \theta_i$  and  $s_e$  and  $s_i$ , with mean maximal firing rates for each population given by  $e_{\max}$  and  $i_{\max}$ .

For numerical solution the system of mixed order ODEs is rewritten as a set of ten nonlinear first order ODEs.

## METHODS

### Numerical solutions of the ordinary differential equations

We solve the system of differential equations using CVODE,<sup>13</sup> a software library written in C. We used the backward differentiation formula (BDF) method implemented by CVODE, with a user-supplied analytic Jacobian matrix, and CVODE’s dense linear solver option. Scalar absolute and relative tolerances of  $10^{-9}$  were used, and the system was integrated for  $10^5$  milliseconds (100 seconds). Numerical experiments showed that this period of time was sufficiently long for the system to converge to a stable estimate of the largest Lyapunov exponent (LLE). Random initial conditions, and, where applicable, random values of  $p_{ee}$  and  $p_{ei}$  for the system were generated using the random number generation library SPRNG.<sup>14</sup>

All numerical solutions were performed on the Swinburne Supercluster, a dedicated network of 64 Compaq Alpha workstations, of the Swinburne Center for Astrophysics and Supercomputing.

### Determination of Lyapunov exponents

In order to determine the LLE we implemented the continuous Gram–Schmidt orthonormalization algorithm of Christiansen and Rugh.<sup>15</sup> This utilizes the Jacobian matrix of the system under investigation to construct an augmented set of ODEs, which when numerically solved, gives the LLE of the system. In our case, the system of ten equations is augmented with an additional eleven first order ODEs. The continuous orthonormalization assists in maintaining numerical accuracy in exponent determination. The algorithm also allows us to derive systems of ODEs to calculate as many of the Lyapunov exponents of the system as we need.

### Attractor reconstruction

The attractors shown were time-delay embedded using the  $h_e$  time series with an embedding delay of 4 milliseconds which happened to coincide with the approximate location of the first zero of the autocorrelation function for each time series. The time series used to generate the delay-time-embedded attractors were created using XPPAUT.<sup>16</sup> Autocorrelations and delay-time embeddings were calculated using software from the TISEAN<sup>17</sup> package.

All attractors are from time series 100 seconds long, following the removal of an initial transient of length 5 seconds. Autonomous attractors were calculated using the CVODE option of XPPAUT, with an output temporal resolution of 1 point per millisecond. For the noise-driven attractor a fourth order Runge–Kutta integrator with a fixed timestep of 0.1 milliseconds was used. Every tenth point is displayed, yielding the same temporal resolution as the autonomous attractors. Two independent, normally distributed noise

sources with the same standard deviations were used to add noise to the system via the  $p_{ee}$  and  $p_{ei}$  terms of Eqs. (3) and (5).

### Attractor dimensions

A method for the approximate determination of the dimension of chaotic attractors from systems of ordinary differential equations is via the Kaplan–Yorke formula,<sup>18,19</sup> which relates the Lyapunov exponents of the system to the dimensionality of the chaotic attractor of the system. The Kaplan–Yorke dimension  $D_{KY}$  (which has been shown to be an upper bound to the correlation dimension<sup>20</sup>), is defined as

$$D_{KY} = j - \frac{\lambda_1 + \lambda_2 + \dots + \lambda_j}{\lambda_{j+1}}, \quad (8)$$

where  $\lambda_1 > \lambda_2 > \dots > \lambda_N$  are the Lyapunov exponents for the system and  $j$  is the largest integer for which  $\lambda_1 + \lambda_2 + \dots + \lambda_j \geq 0$ .

In our case, all chaotic attractors investigated in detail have been found to have  $\lambda_1 > 0$ ,  $\lambda_2 = 0$  and  $|\lambda_1| < |\lambda_3|$  so  $D_{KY}$  simplifies to

$$D_{KY} = 2 - \frac{\lambda_1}{\lambda_3}. \quad (9)$$

In order to calculate the top three Lyapunov exponents for our system we solved a derived system of 43 coupled, non-linear, first order ODEs (see the subsection titled Determination of Lyapunov exponents), using the method discussed above (see the subsection titled Numerical solutions of the ordinary differential equations).

### Fat fractal analysis

In order to determine the fat fractal nature of the set of points in parameter space which support chaotic dynamics, we selected all points in Fig. 1 whose LLE  $\geq 0.1 \text{ s}^{-1}$  base  $e$ , yielding a set of 578 227 points. We then covered this set with squares of variable side length ( $\varepsilon$ ) and calculated the number of squares  $[N(\varepsilon)]$  occupied as a function of  $\varepsilon$ . The area of the covering set is  $\mu(\varepsilon) = N(\varepsilon)\varepsilon^2$ . Umberger and Farmer<sup>21</sup> assume a scaling relation for small  $\varepsilon$  of the form  $\mu(\varepsilon) = \mu_0 + K\varepsilon^\gamma$ , with  $K$  a constant,  $\mu_0$  the limiting measure of the set, and  $\gamma$  the fat fractal exponent. We calculated  $\mu_0$ ,  $K$ , and  $\gamma$  by performing a Levenberg–Marquardt non-linear fit of our model to our data set over the scaling region  $0.02 < \varepsilon < 1.0$ .

## RESULTS

As part of our investigations into the possible types of dynamics the model gives rise to under parametric variation we discovered solutions which showed the typical hallmarks of chaotic behavior, namely complicated, aperiodic time series and broad band spectra. The confirmation of the existence of a positive largest Lyapunov exponent provided a clear quantitative hallmark of chaos for the system under investigation. In addition we examined the extent of chaos under parametric variation and the spatial structure of the region of chaotic behavior in parameter space.

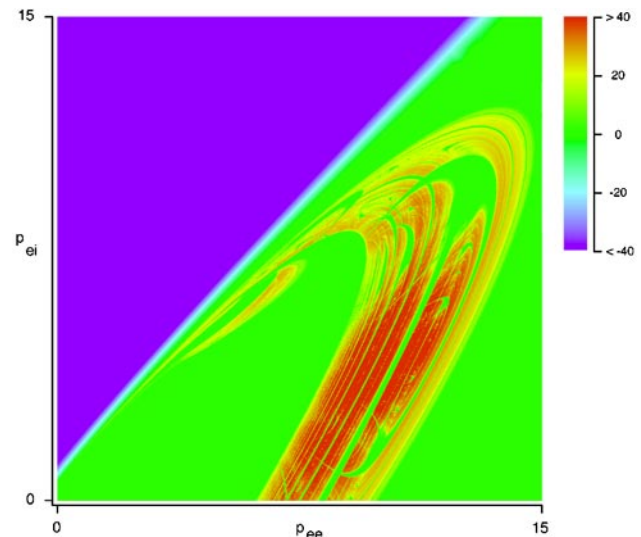


FIG. 1. (Color online) The dependence of the largest Lyapunov exponent of the system on  $p_{ee}$  and  $p_{ei}$ . The parameter space plane depicts the three different dynamical scenarios present in the model, with point attractor, limit cycle, and chaotic dynamics evident. The LLE was determined at each of 1, 201, 310 random locations in this plane (the region containing positive LLEs was more densely sampled than the point attractor and limit cycle regions). LLEs at each point in the figure were obtained by linear interpolation based on a triangulation of the sampled data and mapped according to the key shown. Parameters:  $A = 0.81 \text{ mV}$ ,  $B = 4.85 \text{ mV}$ ,  $a = 490 \text{ s}^{-1}$ ,  $b = 592 \text{ s}^{-1}$ ,  $\tau_e = 9 \text{ ms}$ ,  $\tau_i = 39 \text{ ms}$ ,  $e_{\max} = i_{\max} = 500 \text{ s}^{-1}$ ,  $s_e = s_i = 5 \text{ mV}$ ,  $\theta_e = \theta_i = -50 \text{ mV}$ ,  $N_{ee} = N_{ei} = 3034$ ,  $N_{ie} = N_{ii} = 536$ ,  $h_{er} = h_{ir} = -70 \text{ mV}$ ,  $h_{eeq} = 45 \text{ mV}$ ,  $h_{ieq} = -90 \text{ mV}$ ,  $p_{ie} = 0$ ,  $p_{ii} = 0$ .

Figures 1 and 2 present the results of a detailed investigation into the stability of chaos in a particular parameter set with respect to perturbations in the external excitatory inputs to the excitatory ( $p_{ee}$ ) and inhibitory ( $p_{ei}$ ) neural populations of the model, while keeping the remaining parameters fixed. We investigated variations in  $p_{ee}$  and  $p_{ei}$  since, consistent with physiology, these are the most rapidly and widely fluctuating parameters in the model. Other parameters

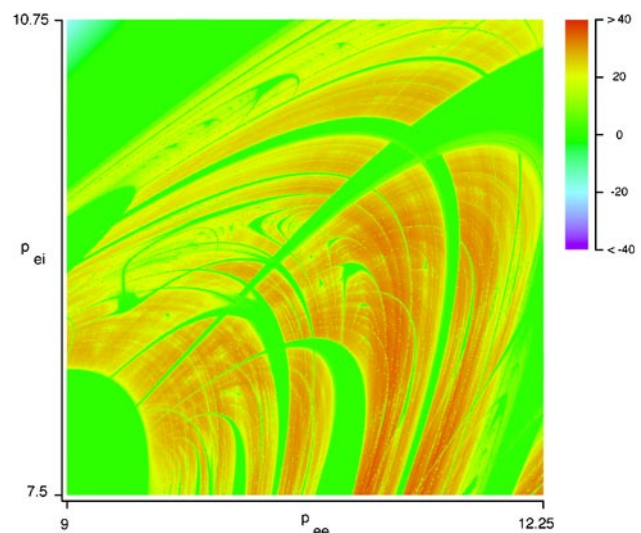


FIG. 2. (Color online) An enlarged view of part of the region supporting chaotic dynamics from Fig. 1. The LLE at each of 841,737 random locations within this square were calculated to produce this plot. Parameters, mapping, and plot creation methods are identical to Fig. 1.

will also vary in time, but such variations are generally several orders of magnitude slower than variations in  $p_{ee}$  and  $p_{ei}$ . The effect of variations in these other parameters will form the focus for future work.

Figure 1 shows, for our particular chaotic parameter set, the effects of varying  $p_{ee}$  and  $p_{ei}$  over the range 0 to 15 afferent pulses per neurone per millisecond.<sup>22</sup> Three distinct dynamical regimes are supported by this parameter space: point attractor dynamics, with a negative LLE; limit cycle dynamics, with a zero LLE; and chaotic dynamics, with a positive LLE.

Figure 2 complements Fig. 1 by showing a more densely sampled view of a region of the chaotic parameter set of Fig. 1. The loops, folds and whirls present in Fig. 1 are also present at increasingly smaller and smaller spatial scales in Fig. 2. This characteristic of repeating spatial structure at smaller and smaller scales indicates that the set of chaotic parameter values for this plane may show some fractal characteristics. Simple fractals like the Cantor set and the Sierpinski gasket, in the limit of smaller and smaller spatial scales, form sets of points of zero measure, where, while existing, they occupy only infinitesimally small areas or volumes, effectively having no area or volume (zero measure) in the limiting case.<sup>23</sup> In the chaotic parameter sets we studied, such limiting behavior is not observed, indicating that we have chaotic parameter sets with positive (finite) measure in parameter space.

Objects which show structure at all scales and which have positive measure are called fat fractals.<sup>23</sup> The application of the Umler–Farmer<sup>21</sup> box-counting method of fat fractal analysis to our chaotic parameter set showed convergence over a two decade scaling region. The set shown in Fig. 1 has a fat fractal exponent of approximately 0.5, suggesting an object of some fat fractal structure in a set of evident positive measure.

The dynamics corresponding to the chaotic points in this plane are consistent with that of gamma band EEG, with peak spectral power overwhelmingly within the 30–100 Hz frequency band.<sup>24</sup> There are also significant areal variations in the LLE within this plane. Figures 3(a) and 3(b) show embeddings of attractors from two different locations in the plane. The attractor in Fig. 3(a) has a LLE of 5.51 ( $N=25$ , SD 0.08)  $s^{-1}$  base  $e$ , compared to the attractor in Fig. 3(b) which has a LLE of 42.9 ( $N=25$ , SD 0.4)  $s^{-1}$  base  $e$ . The attractors have different detail, but share an overall familial similarity in their broadly tricuspid nature and in their flow profiles.

The attractor of Fig. 3(a) has a Kaplan–Yorke (or Lyapunov) dimension of 2.0163 ( $N=25$ , SD 0.0002), and the attractor of Fig. 3(b) has a Kaplan–Yorke dimension of 2.0933 ( $N=25$ , SD 0.0007). While the LLE values of attractors may differ greatly, their overall skeletal structure and dimensionality remain broadly similar. The effects of noise in  $p_{ee}$  and  $p_{ei}$  will cause any fine structure of individual attractors to smear out, but, as the examples shown in Figs. 3(c) and 3(d) indicate, the familial structure of the attractors is preserved.

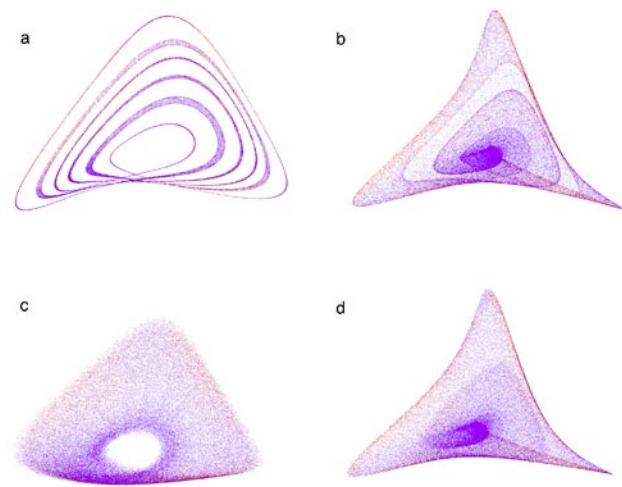


FIG. 3. (Color online) Delay-embedded  $h_e$  time series attractors, varying  $p_{ee}$  and  $p_{ei}$ . All other parameters are identical to Fig. 1. (a) Autonomous attractor with  $p_{ee}=12.9$ ,  $p_{ei}=11.9$ . Averaged over 25 simulations, the top three Lyapunov exponents ( $s^{-1}$  base  $e$ ) for this particular attractor are  $\lambda_1 = 5.50$  (SD 0.08),  $\lambda_2 = -0.01$  (SD 0.01) and  $\lambda_3 = -337.18$  (SD 0.08), with a Kaplan–Yorke dimension of 2.0163 (SD 0.0002). (b) Autonomous attractor for  $p_{ee}=10$  and  $p_{ei}=4$ . Averaged over 25 simulations, the top three Lyapunov exponents for this particular attractor are  $\lambda_1=42.9$  (SD 0.4),  $\lambda_2 = -0.01$  (SD 0.02), and  $\lambda_3 = -459.9$  (SD 0.4), with a Kaplan–Yorke dimension of 2.0933 (SD 0.0007). (c) Noise driven attractor, with mean  $p_{ee}$  and  $p_{ei}$  as in (a) and normally distributed white noise, with standard deviation 0.316 added to each population input (see the subsection entitled Attractor reconstruction). (d) Noise driven attractor, with mean  $p_{ee}$  and  $p_{ei}$  as in (b) and noise standard deviation as in (c).

## DISCUSSION

Based on his extensive studies of the mammalian olfactory system, Freeman suggested that chaos plays a central role in the ability of sensory systems to respond in a rapid and unique fashion to different perceptual stimuli.<sup>1,2,25</sup>

On the basis of his careful experimental and theoretical studies, Freeman concludes that the olfactory system uses bursts of chaotic gamma band activity to signify the perception of the odor to the animal. He considers the details of the chaotic behavior of this signal to be both stimulus- and context-dependent, with the chaotic attractor for this signal a representation of the particular odor, and emphasizes that these attractors, together with their basins of attraction, are not invariant representations. The learning of a novel odor leads to the creation of a new representative attractor together with a new basin of attraction, as well as the simultaneous modification of the preexisting attractors and their respective basins of attraction.

A common experience for many of us involves the recognition and acknowledgment of a particular odor, even “before we have had time to think.” This notion of preattentive perception, i.e., the perception of a stimulus before we have even formally focused our attention to it, implies that the brain must use a flexible and rapid system for the perception of stimuli. In other words, it becomes important for the brain to be able to easily, reliably, and quickly, switch between different dynamical scenarios. Freeman believes transitions between different dynamical scenarios can be considered as either bifurcations, or phase transitions, in a noisy environ-

ment. Brains rapidly select either a preexisting attractor, or commence the creation of a new attractor and basin, depending on the form of the presented stimulus. The concept of random transitions between states does not fit in with Freeman's experimental findings or theoretical predictions.<sup>2</sup> Having a basal state for the brain which is predominantly chaotic, which allows for the rapid transition between attractors or the creation of new attractors, by small changes in the brain's input, is therefore a natural conclusion.

Freeman therefore considers that chaos is the most probable mechanism that underpins the major perceptual processes, consistent with his experimental and theoretical analyses of palaeocortical and neocortical neurodynamics. We consider that the work presented herein is consistent with Freeman's theoretical developments, and suggest that our work is now amenable to the construction of a similar analogy.

Instead of considering the selection of chaotic attractors as the selection of attractors from individual loci from within the plane of Fig. 1, the selection may occur by choosing individual regional attractors from the plane. Because, over any small region of the plane, the essential familial structure of an attractor remains the same (possibly due to the finite measure of chaos within the space), the noise, instead of complicating matters by removing our ability to select individual attractors from within the plane, helps to create prototypical attractors for a region, which under synaptic modification and other forms of neuromodulation, may change akin to Freeman's suggestion. Thus Freeman's attractors may be the archetypal noisy attractors of small regions of parameter space, each selectable by modification by the system of some combination of parameters.

The human neocortex can be considered to consist of many thousands of macrocolumns. If each neocortical macrocolumn operates in a noisy, chaotic mode, coupled to many other macrocolumns via short and long range connections, then with one scalp electrode recording the electrical activity of up to 6 cm<sup>2</sup> of brain tissue and given the rapid variation of the LLEs with changing parameter values, it is reasonable to conclude that an attempt to use scalp recorded EEG data to look for chaotic dynamics in the brain is unlikely to succeed. The electroencephalogram is now neither completely noisy, nor completely chaotic, but it does definitely have an underlying chaotic basis. This chaotic base state, combined with

the omnipresent noise in the brain, means that the electroencephalogram has structure consistent with that of Freeman's notion of stochastic chaos.<sup>24</sup>

## ACKNOWLEDGMENTS

M.P.D. is supported by an Australian Postgraduate Award. The authors thank Paul Bourke for his advice and assistance with the preparation of the graphics in this paper, Professor Matthew Bailes for computational support, and Associate Professor Tim Hendtlass for his careful reading of the manuscript.

- <sup>1</sup>W. J. Freeman, in *Neural Networks and Neural Modeling*, edited by F. Ventriglia (Pergamon, New York, 1994), p. 185.
- <sup>2</sup>W. J. Freeman, *Sci. Am.* **264**, 34 (1991).
- <sup>3</sup>W. J. Freeman and J. M. Barrie, in *Temporal Coding in the Brain*, edited by G. Buzsaki, R. Llinas, W. Singer, A. Berthoz, and Y. Christen (Springer-Verlag, Berlin, 1994), p. 13.
- <sup>4</sup>P. L. Nunez, *Behav. Brain Sci.* **23**, 371 (2000).
- <sup>5</sup>A. van Rotterdam, F. H. Lopes da Silva, J. van den Ende, and A. J. Hermans, *Bull. Math. Biol.* **44**, 283 (1982).
- <sup>6</sup>V. K. Jirsa and H. Haken, *Physica D* **99**, 503 (1997).
- <sup>7</sup>J. J. Wright and R. R. Kydd, *Network* **3**, 341 (1992).
- <sup>8</sup>P. A. Robinson, C. J. Rennie, and J. J. Wright, *Phys. Rev. E* **56**, 826 (1997).
- <sup>9</sup>W. S. Pritchard, in *Analysis of the Electrical Activity of the Brain*, edited by F. Angeleri, S. Butler, S. Giaquinto, and J. Majkowski (Wiley, Chichester, 1997), p. 3.
- <sup>10</sup>P. L. Nunez, *Electric Fields of the Brain* (Oxford University Press, New York, 1981).
- <sup>11</sup>R. Cooper, A. L. Winter, H. J. Crow, and W. Grey Walter, *Electroencephalogr. Clin. Neurophysiol.* **18**, 217 (1965).
- <sup>12</sup>D. T. J. Liley, P. J. Cadusch, and J. J. Wright, *Neurocomputing* **26–27**, 795 (1999).
- <sup>13</sup>S. D. Cohen and A. C. Hindmarsh, *Comput. Phys.* **10**, 138 (1996).
- <sup>14</sup>M. Mascagni, in *Algorithms for Parallel Processing*, edited by M. T. Heath, A. Ranade, and R. S. Schreiber (Springer-Verlag, New York, 1999), p. 277.
- <sup>15</sup>F. Christiansen and H. H. Rugh, *Nonlinearity* **10**, 1063 (1997).
- <sup>16</sup>G. B. Ermentrout, XPPAUT, <http://www.pitt.edu/~phase>.
- <sup>17</sup>R. Hegger, H. Kantz, and T. Schreiber, *Chaos* **9**, 413 (1999).
- <sup>18</sup>J. L. Kaplan and J. A. Yorke, in *Functional Differential Equations and Approximation of Fixed Points*, edited by H-O. Peitgen and H-O. Walther (Springer-Verlag, Berlin, 1979), p. 204.
- <sup>19</sup>J. D. Farmer, E. Ott, and J. A. Yorke, *Physica D* **7**, 153 (1983).
- <sup>20</sup>P. Grassberger and I. Procaccia, *Physica D* **9**, 189 (1983).
- <sup>21</sup>D. K. Umberger and J. D. Farmer, *Phys. Rev. Lett.* **55**, 661 (1985).
- <sup>22</sup>W. J. Freeman, *Societies of Brains* (Lawrence Erlbaum Associates, Mahwah, 1995).
- <sup>23</sup>R. Eykholt and D. K. Umberger, *Physica D* **30**, 43 (1988).
- <sup>24</sup>W. J. Freeman, *Neural Networks* **13**, 11 (2000).
- <sup>25</sup>W. J. Freeman, *Int. J. Bifurcation Chaos Appl. Sci. Eng.* **2**, 451 (1992).